Structure and Magnetism of a Bimetallic Pentanuclear Cluster $[(Ni(bpm)_2)_3(Fe(CN)_6)_2]\cdot 7H_2O$ (bpm = Bis(1-pyrazolyl)methane)). The Role of the Hydrogen-Bonded $7H_2O$ "Cluster" in Long-Range Magnetic Ordering

Kenneth Van Langenberg,[†] Stuart R. Batten,[†] Kevin J. Berry,[‡] David C. R. Hockless,[§] Boujemaa Moubaraki,[†] and Keith S. Murray*,[†]

Chemistry Department, Monash University, Clayton, Victoria 3168, Australia, Westernport Secondary College, Hastings, Victoria 3915, Australia, and Research School of Chemistry, The Australian National University, Canberra, ACT 0200, Australia

Received February 12, 1997[⊗]

The synthesis and structural and magnetic properties of the pentanuclear complex $[(Ni(bpm)_2)_3(Fe(CN)_6)_2]\cdot 7H_2O$ (**1**) are reported. Complex **1** crystallizes in the tetragonal space group $P4_32_12$ (No. 96) with the following cell parameters at 23(1) °C: $a = b = 12.888(2)$ Å, $c = 42.927(2)$ Å, $V = 7130(3)$ Å^3, and $Z = 4$. The structure was refined using 3197 unique reflections with $I > 3\sigma(I)$ to give $R = 0.047$ and $R_w = 0.038$. The neutral $[(Ni(bpm)_2)_3(Fe(CN)_6)_2]$ clusters contain two unconnected $Fe^{III}(CN)_6^{3-}$ groups each bridged, via three facial CN groups, to three *cis*-$Ni(bpm)_2$ moieties, thus making the *cis*-$(CN)_2Ni^{II}(bpm)_2$ centers six-coordinate. Metal···metal distances within the cluster are Fe···Ni = 5.042(3) and 5.058(2) Å, Fe···Fe = 6.438(4) Å, and Ni···Ni = 6.654(3) and 7.028(5) Å. The seven water molecules form an intriguing hydrogen-bonded "cluster" which connects, via hydrogen-bonding, to the other facial CN ligands on each Fe. A wide array of magnetic susceptibility and magnetization measurements has been used to show that the Ni_3Fe_2 clusters display intramolecular ferromagnetic coupling. Most importantly, the crystalline samples of **1** and most, but not all, of rapidly precipitated powder samples display long-range magnetic ordering with $T_c = 23$ K. The powder samples which do not display magnetic order yield X-ray diffraction patterns, IR spectra, and thermogravimetric behavior identical to those of samples that display magnetic order. Experimental attempts to identify the nature of the magnetic phase transition in the ordered samples of **1** lead to ferromagnetic ordering being favored over spin-glass formation. The $7H_2O$ hydrogen-bonded moiety plays a key role in intercluster exchange interactions. Dehydrated samples of **1** are not ordered. Intracluster exchange interactions are deduced for the dehydrated form.

Introduction

Since our preliminary report[1] on "molecular" cyano-bridged bimetallic species of stoichiometry $[A^{II}(chelate)_n]_3[B^{III}(CN)_6]_2\cdot xH_2O$ and those on related species by Okawa *et al.*[2,3] and Matsumoto *et al.*,[4−7] there have been further recent reports by Verdaguer *et al.*,[8] Gatteschi *et al.*,[9] and Smekal *et al.*[10,11] on compounds possessing similar stoichiometry, some of which are magnetically ordered. The structures of such materials are fascinating and varied and all have B−CN−A bridges held within various extended motifs. For instance, $[Ni(en)_2]_3[Fe(CN)_6]_2\cdot 2H_2O$ (en = 1,2-diaminoethane) and $[Ni(pn)_2][Fe(CN)_6]ClO_4\cdot 2H_2O$ (pn = 1,2-diaminopropane) have chain (rope−ladder) and 2-D sheet structures, respectively.[2,3] The complex $[Ni(cyclam)]_3[Cr(CN)_6]_2\cdot 20H_2O$ (cyclam = 1,4,8,11-tetraazacyclotetradecane) has a layered structure with corrugated sheets[8] while $[Ni(tren)]_3[Fe(CN)_6]_2\cdot 6H_2O$ (tren = tris(2-aminoethyl)amine) has a 3D structure consisting of ···Fe−CN−Ni−NC−Fe−CN··· chains running parallel to the three cell axes.[9] 2-D layer structures have also been observed in bimetallic Mn^{III}−Schiff base hexacyanometalates of the type $K[Mn^{III}(3\text{-MeOsalen})]_2[Fe(CN)_6]$ (3-MeOsalen = *N*,*N*′- ethylene(3-methoxysalicylideneaminato) dianion).[5] Long-range magnetic ordering involving ferro-, ferri-, and metamagnetism has been observed, and relationships to structure have been sought.

While not always explicitly discussed, the physical nature of the solid samples used for magnetic measurements, i.e. powder/polycrystalline versus collection of single crystals, probably plays an important role in the observed magnetization data.[5] Thus, the initial claim of metamagnetic ordering in $[Ni(en)_2]_3[Fe(CN)_6]_2\cdot 2H_2O$[2] appears now to apply only to a polycrystalline form, the reported magnetization data being dependent on sample preparation method and crystallite size.[12] The Ni(pn)

* Corresponding author. Fax: 61-3-9905-4597.
[†] Monash University.
[‡] Westernport Secondary College.
[§] The Australian National University.
[⊗] Abstract published in *Advance ACS Abstracts,* September 15, 1997.

(1) Murray, K. S.; Fallon, G. D.; Hockless, D. C. R.; Lu, K. D.; Moubaraki, B.; Van Langenberg, K. In *Molecule-Based Magnetic Materials*; Turnbull, M. M., Sugimoto, T., Thompson, L. K., Eds.; ACS Symposium Series 644; American Chemical Society: Washington, DC, 1996; Chapter 13, pp 201−215.
(2) Ohba, M.; Maruono, N.; Okawa, H.; Enoki, T.; Latour, J.-M. *J. Am. Chem. Soc.* **1994**, *116*, 11566.
(3) Ohba, M.; Okawa, H. *Mol. Cryst. Liq. Cryst. Sci. Technol., Sect. A* **1996**, *285*, 423.
(4) Miyasaka, H.; Matsumoto, N.; Okawa, H.; Re, N.; Gallo, E.; Floriani, C. *Angew Chem., Int. Ed. Engl.* **1995**, *34*, 1446.
(5) Miyasaka, H.; Matsumoto, N.; Okawa, H.; Re, N.; Gallo, E.; Floriani, C. *J. Am. Chem. Soc.* **1996**, *118*, 981.
(6) Re, N.; Gallo, E.; Floriani, C.; Miyasako, H.; Matsumoto, N. *Inorg. Chem.* **1996**, *35*, 6004.
(7) Re, N.; Gallo, E.; Floriani, C.; Miyasaka, H.; Matsumoto, N. *Inorg. Chem.* **1996**, *35*, 5964.
(8) Ferlay, S.; Mallah, T.; Vaissermann, J.; Bartalomé, F.; Veillet, P.; Verdaguer, M. *Chem. Commun.* **1996**, 2481.
(9) Salah El Fallah, M.; Rentschler, E.; Caneschi, A.; Sessoli, R.; Gatteschi, D. *Angew. Chem., Int. Ed. Engl.* **1996**, *35*, 1947.
(10) Smekal, Z.; Brezina, F.; Sindelar, Z.; Klicka, R.; Krausova, D.; Nadvornik, M. *Synth. React. Inorg. Met. Org. Chem.* **1996**, *26*, 1537.
(11) Smekal, Z.; Brezina, F.; Sindelar, Z.; Klicka, R.; Krausova, D.; Nadvornik, M. *Pol. J. Chem.* **1996**, *70*, 725.
(12) Ohba, M.; Pukita, N.; Okawa, H. *J. Chem. Soc., Dalton Trans.* **1997**, 1733.

S0020-1669(97)00160-2 CCC: $14.00

complex is a metamagnet[3] as is the $Mn(3\text{-MeOsalen})^+$ adduct, the latter being studied in both powder and crystalline forms.[5]

The role of the water molecules in some of these multihydrated species is even less clear. Thus the powder sample of formula $[Ni(cyclam)]_3[Cr(CN)_6]_2 \cdot 5H_2O$ does not show bulk ordering down to 2 K, but rather ferromagnetic short-range coupling with a $\chi_M T$ vs T plot typical of that expected for a $Ni^{II}{}_3Cr^{III}{}_2$ repeat unit. Unfortunately, the magnetism of the parent crystal structure $[Ni(cyclam)]_3[Cr(CN)_6]_2 \cdot 20H_2O$ could not be determined because of ready loss of water molecules, the latter occupying the interlayer spaces and forming a network of hydrogen bonds. The lattice structures of the $5H_2O$ and $20H_2O$ species were assumed similar.[8] Kahn *et al*. had earlier noted the influence of the degree of hydration on the type of magnetic order in $Cu^{II}Mn^{II}$ oxamide systems.[13]

In this paper, we report the crystal structure of a new type of bimetallic hexacyanoferrate(III) motif found in the 3:2 complex $[(Ni(bpm)_2)_3(Fe(CN)_6)_2] \cdot 7H_2O$, **1** (bpm = bis(1-pyrazolyl)-methane). In contrast to the Ni^{II} and Mn^{III} chelated compounds, discussed above, having infinite 2-D sheet- or chainlike cyano-bridged components, complex **1** forms discrete pentanuclear clusters, each cluster being connected to neighboring clusters in the crystal lattice via a novel hydrogen-bonded "cluster" of seven water molecules. Detailed susceptibility, magnetization, and hysteresis studies are described in order to try to identify the nature of the long-range ordering and concomitant magnetic phase transition which occurs in some samples of **1** at a T_c value of *ca*. 23 K. The possibility of spin-glass formation is discussed briefly and is rejected on experimental and structural grounds. The effects of sample preparation and crystallite size on the magnetic properties are discussed, as are attempts to identify the role of the H-bonded water molecules in transmitting intercluster interactions. We recently showed that the bipyridine analog $[(Ni^{II}(bipy)_2)_3(Fe(CN)_6)_2] \cdot 7H_2O$ (bipy = 2,2′-bipyridine) contains the same pentanuclear cluster as found in **1**, but with a different crystal space group. It also displays long-range ordering.[14]

In a more general sense, studies of clusters of type **1** add to the growing knowledge on new molecular magnetic materials based on cluster structures, particularly those displaying large spin ground states and large molecular anisotropy.[15−19] An important current example is $[Mn_{12}O_{12}(OAc)_{16}(H_2O)_4] \cdot 2HOAc \cdot 4H_2O$, which displays unusual quantum magnetic hysteresis originating from *within* each cluster rather than from cooperative effects between neighboring cluster molecules.[17,19]

Experimental Section

General Details. All chemicals and reagents were used as received. Bis(1-pyrazolyl)methane (bpm) was prepared according to published procedures.[20]

Infrared spectra were measured on a Perkin-Elmer 1600 FT-IR instrument with samples contained as Nujol mulls between NaCl plates. The ν(CN) region was expanded. Microanalyses (C, H, N) were performed by the Commonwealth Micro-analytical Services Pty Ltd., Melbourne. Thermogravimetric analyses (TGA) were performed with a Stanton-Redcroft STA-780 Seneg thermal analyzer using 12 mg of Al_2O_3 as the reference sample and compressed air as the atmosphere. Powder X-ray diffraction profiles were recorded on a Scintag automated powder diffractometer using Cu Kα radiation, a solid state detector, a 2 mm divergence slit, and a 3 mm receiving slit. The fractional coordinates and space group of the crystal structure of **1** were used to calculate the peak position of the XRD profile. The observed diffractograms for all of the powdered samples were then compared to the calculated positions. In one case, sample 3, the cell constants were refined in the space group $P4_32_12$ and were identical to those of the crystal structure.

Magnetic susceptibility and magnetization measurements were made using a Quantum Design MPMS5 SQUID magnetometer. Samples were contained within gelatine capsules (for 1 T field work) or quartz tubes (for low-field work). The usual measuring protocol for low-field work was to cool the samples in a field of 5 Oe from 35 to 4.2 K while the magnetization (FCM) was recorded. For ZFCM measurements, the sample was cooled in zero field and then warmed in a field of 5 Oe while measurements were made. Remanent magnetization (RM) measurements were made by turning the field to zero at the lowest temperature and then recording the RM values upon warming. The magnetization data in the range 0−5 T for samples 1 and 3 were obtained by starting at zero field, with a fixed temperature (e.g., 2 K), and then increasing the field to various values up to 5 T; the temperature was then changed to, e.g., 3 K, and the fields were varied from 5 T, 4 T, ... to zero prior to changing the temperature and increasing the field once again. This protocol is fine for fields greater than the coercive field value, e.g., for high-field saturation studies, but may suffer from hysteresis/domain movement effects on the line shape at very low field values.

Preparation of $[Ni(bpm)_2(H_2O)_2](NO_3)_2$. Solid bpm (2.96 g, 20 mmol) was added to a stirred solution of $Ni(NO_3)_2 \cdot 6H_2O$ (2.91 g, 10 mmol) in water (100 mL). The ligand dissolved completely after approximately 15 min, resulting in a deep blue homogeneous solution. This solution was allowed to slowly evaporate over a period of days to give well-formed blue crystals. These were collected by filtration, washed with small amounts of water and diethyl ether, and dried in air. Yield: 4.3 g (84%). Anal. Calcd for $C_{14}H_{20}N_{10}O_8Ni$: C, 32.6; H, 3.9; N, 27.2. Found: C, 32.4; H, 4.1; N, 29.2.

Preparation of Complex 1, $[(Ni(bpm)_2)_3(Fe(CN)_6)_2] \cdot 7H_2O$. (a) Rapid Precipitation in Water. To a solution of $[Ni(bpm)_2(H_2O)_2](NO_3)_2$ (0.77 g, 1.5 mmol) in 50 mL of water was added dropwise, with rapid stirring, a solution of $K_3Fe(CN)_6$ (0.33 g, 1 mmol) in water (50 mL). This led to the immediate precipitation of a fine yellow solid. The mixture was centrifuged to recover the yellow solid, which was then washed with water and centrifuged. This procedure was repeated, and the yellow solid was left to dry in air overnight. Anal. Calcd for $C_{54}H_{62}N_{36}O_7Ni_3Fe_2$: C, 40.2; H, 3.9; N, 31.2. Found: C, 40.0; H, 3.9; N, 31.3. IR (Nujol): 2173, 2164, 2151, 2125, 2116 cm^{-1}; ν(C≡N). The above method of synthesis and isolation, employing a 3:2 nickel to iron mole ratio, refers to most of the samples prepared. In two cases, including sample 3, a 1:1 mole ratio of reagents was used.

(b) Single Crystals (Samples 1 and 2). A solution of $K_3Fe(CN)_6$ (0.08 g, 0.25 mmol) in 2-propanol/water (1:1 v/v, 30 mL of mixed solution) was allowed to diffuse through the glass frit of an H-tube into a solution of $[Ni(bpm)_2(H_2O)_2](NO_3)_2$ (0.13 g, 0.25 mmol) in DMF (30 mL). After several weeks in the dark, well shaped, yellow-orange crystals were obtained.

Structure Determination of 1. Orange prisms of **1** were grown as described above, and a crystal of dimensions 0.12 × 0.12 × 0.10 mm was employed. Data were collected using a Rigaku AFC 6R diffractometer equipped with a rotating anode and graphite-monochromated Cu Kα radiation. Cell dimensions and intensities were measured by $\omega-2\theta$ scans. A total of 5971 reflections were scanned in the range $3 < 2\theta < 120.1°$, with $0 < h < 14$, $0 < k < 14$, and $0 < l < 48$, and of these, 3197 reflections were unique ($R_{int} = 0.116$). A total of 1404 reflections were considered observed, having $I > 3\sigma(I)$, and used in the final cycle of the structure solution and refinement. Data were

(13) Pei, Y.; Kahn, O.; Nakatoni, K.; Codjovi, E.; Mathoniere, C.; Sletten, J. *J. Am. Chem. Soc.* **1991**, *113*, 6558.
(14) Van Langenberg, K.; Hockless, D. C. R.; Moubaraki, B.; Murray, K. S. Unpublished data.
(15) Gatteschi, D.; Caneschi, A.; Pardi, L.; Sessoli, R. *Science* **1994**, *265*, 1054.
(16) Gatteschi, D. *Adv. Mater*. **1994**, *6*, 635.
(17) Chudnosky, E. M. *Science* **1996**, *274*, 938.
(18) Squire, R. C.; Aubin, S. M. J.; Folting, K.; Streib, W. E.; Christou, G.; Hendrickson, D. N. *Inorg. Chem.* **1995**, *34*, 6463.
(19) Sessoli, R.; Tsai, H.-L.; Schake, A. R.; Wang, S.; Vincent, J. B.; Folting, K.; Gatteschi, D.; Hendrickson, D. N. *J. Am. Chem. Soc.* **1993**, *115*, 1804.
(20) Elguero, J.; Ochoa, C.; Julia, S.; Sala, P.; Mazo, J.; Sancho, M. *J. Heterocycl. Chem.* **1982**, *19*, 114.

Table 1. Crystallographic Data for $[(Ni(bpm)_2)_3(Fe(CN)_6)_2]\cdot 7H_2O$, **1**

empirical formula	$C_{54}H_{55}Fe_2N_{36}O_7Ni_3$	crystal system	tetragonal
fw	1608.1	T	23.2 °C
space group	$P4_32_12$ (No. 96)	λ	1.541 78 Å
a	12.888(2) Å	ρ_{calc}	1.498 g cm^{-3}
b	12.888(2) Å	μ(Cu Kα)	46.86 cm^{-1}
c	42.927(2) Å	R^a	0.047
V	7130(3) Å^3	$R_w{}^b$	0.038
Z	4	range of transm factors	0.90−1.00

^{a} $R = \sum||F_o| - |F_c||/\sum|F_o|$. ^{b} $R_w = [\sum w(|F_o| - |F_c|)^2/\sum w|F_o|^2]^{0.5}$.

corrected for absorption.[21] Three standard reflections measured after every 150 reflections showed no significant variation in intensity. The space group $P4_32_12$ (No. 96) was not unambiguous.

The structure was solved by direct methods and refined[22,23] by full-matrix least-squares analysis on F using the teXsan Structure Analysis Software of the Molecular Structure Corp.[24] Refinement converged at $R = 0.047$ ($R_w = 0.038$), GOF = 1.55. Crystal data are given in Table 1, and the final atomic coordinates (excluding those for hydrogen atoms) are listed in Table 2. All non-carbon and hydrogen atoms were refined with anisotropic thermal parameters. Carbons were refined isotropically, and hydrogens were included in the refinement at calculated positions and held fixed. The handedness of the molecule was clearly seen after refinement in each enantiomorph. Neutral-atom scattering factors were taken from Cromer and Waber.[25] Anomalous dispersion effects were included in F_c,[26] and the values for $\Delta f'$ and $\Delta f''$ were those of Creagh and McAuley.[27] The values for the mass attenuation coefficients are those of Creagh and Hubbell.[28]

Results and Discussion

Mixing aqueous solutions of $[Ni(bpm)_2(H_2O)_2](NO_3)_2$ and $K_3[Fe(CN)_6]$ in either a 3:3 or 3:2 mole ratio leads to immediate precipitation of a yellow-orange powder of formula $[(Ni(bpm)_2)_3(Fe(CN)_6)_2]\cdot 7H_2O$. XRD measurements on these microcrystalline powders show that they are isostructural with the single-crystal samples and have the same unit cell. The crystals are grown over several weeks by allowing a DMF solution of the nickel salt to diffuse, in the dark, into a solution of $K_3[Fe(CN)_6]$ in 2-propanol/water (1:1 vol/vol). The ν(CN) region of the IR spectrum of the powders shows five bands which are assigned to bridging-CN frequencies at 2173 and 2154 cm^{-1} and terminal frequencies at 2125 and 2116 cm^{-1}, the latter arising from terminal CN groups which form weak hydrogen bonds to lattice water (see below). A band at 2164 cm^{-1} is assigned to the terminal C−N(4) group which forms a strong H-bond with O(4). The IR spectra of crystalline samples are identical to those of powder samples.

Powder or crystalline samples were stable over long periods under ambient laboratory conditions and showed reproducible magnetic data over such time periods. Thermogravimetric studies of the powder samples are all extremely similar in the 25−800 °C region and show a weight loss of 9.0 ± 0.3% in the temperature range 30−160°, corresponding to the loss of eight molecules of water. Microanalytical data, given in the Experimental Section, cannot distinguish $8H_2O$ from the $7H_2O$ found in the crystal structure of sample 1. There are further weight losses from 250 °C until 400 °C which can be attributed to the loss of ligand molecules and cyanide, though there appears to be some overlap of the two processes. When the material was carefully heated under N_2 to 200 °C for 36 h to remove all of the water molecules, the anhydrous product remained microcrystalline as judged by the sharp XRD. The diffractogram has a different 2θ pattern compared to that of the parent hydrate. In the IR spectrum, the bridging ν(CN) frequencies at 2173 and 2156 cm^{-1} are the same as those for the hydrate.

Table 2. Atomic Coordinates and B_{eq} Values for **1**

atom^a	x	y	z	B_{eq},^{b} Å^2
Ni(1)	0.1524(2)	0.9258(2)	0.06624(6)	3.19(7)
Ni(2)	0.3490	1.3490	0.0000	2.61(6)
Fe(1)	0.2804(2)	0.9911(2)	−0.04300(5)	2.50(6)
O(1)	0.926(3)	0.9256	0.0000	13.9(7)
O(2)	0.300(1)	0.845(1)	0.2637(3)	10.8(5)
O(3)	0.263(1)	0.007(1)	0.5287(3)	13.3(6)
O(4)	0.277(1)	0.951(1)	0.5984(3)	8.8(5)
N(1)	0.1784(8)	0.9194(9)	0.0187(2)	3.1(3)
N(2)	0.3413(9)	1.1991(8)	−0.0133(2)	2.8(3)
N(3)	0.0706(9)	1.0859(9)	−0.0610(2)	3.3(3)
N(4)	0.238(1)	0.7821(9)	−0.0743(3)	5.0(4)
N(5)	0.371(1)	1.091(1)	−0.1014(3)	4.9(4)
N(6)	0.493(1)	0.9006(9)	−0.0247(3)	4.4(4)
N(7)	0.209(1)	0.772(1)	0.0723(3)	4.6(4)
N(8)	0.153(1)	0.689(1)	0.0613(3)	5.2(4)
N(9)	−0.009(1)	0.762(1)	0.0560(3)	5.1(4)
N(10)	0.007(1)	0.861(1)	0.0650(3)	4.6(4)
N(11)	0.146(1)	0.936(1)	0.1160(3)	4.3(4)
N(12)	0.204(1)	1.005(1)	0.1321(3)	5.6(5)
N(13)	0.340(1)	1.033(1)	0.0954(3)	5.3(4)
N(14)	0.3027(9)	0.9819(9)	0.0705(3)	3.6(3)
N(15)	0.3947(8)	1.3142(9)	0.0459(2)	3.1(3)
N(16)	0.491(1)	1.276(1)	0.0541(3)	3.7(3)
N(17)	0.585(1)	1.3082(9)	0.0065(2)	3.5(3)
N(18)	0.5085(9)	1.3571(9)	−0.0111(3)	3.4(3)
C(1)	0.217(1)	0.945(1)	−0.0046(3)	2.5(3)
C(2)	0.317(1)	1.122(1)	−0.0223(3)	2.5(3)
C(3)	0.147(1)	1.051(1)	−0.0548(3)	2.3(3)
C(4)	0.250(1)	0.862(1)	−0.0631(3)	3.1(4)
C(5)	0.336(1)	1.050(1)	−0.0805(3)	3.4(3)
C(6)	0.414(1)	0.935(1)	−0.0314(3)	3.5(4)
C(7)	0.281(1)	0.734(1)	0.0914(4)	5.7(5)
C(8)	0.267(2)	0.628(2)	0.0931(4)	7.0(5)
C(9)	0.189(2)	0.602(2)	0.0741(5)	6.7(5)
C(10)	0.070(1)	0.703(1)	0.0395(4)	5.3(4)
C(11)	−0.108(2)	0.732(2)	0.0616(5)	7.3(6)
C(12)	−0.158(1)	0.813(2)	0.0760(4)	6.9(5)
C(13)	−0.084(2)	0.891(1)	0.0774(4)	6.6(5)
C(14)	0.107(1)	0.873(1)	0.1369(4)	5.0(4)
C(15)	0.143(1)	0.898(1)	0.1665(3)	4.6(4)
C(16)	0.204(1)	0.980(1)	0.1635(4)	6.2(5)
C(17)	0.264(2)	1.081(2)	0.1158(4)	6.3(5)
C(18)	0.440(2)	1.033(2)	0.0963(4)	6.9(6)
C(19)	0.483(2)	0.982(2)	0.0709(5)	8.4(6)
C(20)	0.390(1)	0.952(1)	0.0560(4)	5.3(5)
C(21)	0.356(1)	1.341(1)	0.0730(4)	4.5(4)
C(22)	0.427(1)	1.328(1)	0.0978(3)	4.7(4)
C(23)	0.508(1)	1.285(1)	0.0851(4)	5.7(4)
C(24)	0.554(1)	1.234(1)	0.0294(4)	3.9(4)
C(25)	0.676(1)	1.350(1)	0.0006(4)	4.7(4)
C(26)	0.668(1)	1.423(1)	−0.0207(4)	5.3(4)
C(27)	0.560(1)	1.427(1)	−0.0277(4)	4.6(4)

^{a} Occupancy of Ni(2) and O(1) is $^1/_2$. ^{b} $B_{eq} = {}^8/_3\pi^2[U_{11}(aa^*)^2 + U_{22}(bb^*)^2 + U_{33}(cc^*)^2 + 2U_{12}(aa^*bb^*)\cos\gamma + 2U_{13}(aa^*cc^*)\cos\beta + 2U_{23}(bb^*cc^*)\cos\alpha]$.

(21) North, A. C. T.; Phillips, D. C.; Mathews, F. S. *Acta Crystallogr.* **1968**, *124*, 351.
(22) Altomare, A.; Cascarano, M.; Giacovazzo, C.; Guagliardi, A. SIR 92. *J. Appl. Crystallogr.* **1993**, *26*, 343.
(23) Buerskens, P. T.; Admiraal, G.; Buerskens, G.; Bosman, W. P.; de Gelder, R.; Israel, R.; Smits, J. M. M. *The DIRDIF-94 program system*; Technical Report; Crystallography Laboratory, University of Nijmegen: Nijmegen, The Netherlands, 1994.
(24) *teXsan: Crystal Structure Analysis Package*; Molecular Structure Corp.: The Woodlands, TX, 1985 and 1992.
(25) Cromer, D. T.; Waber, J. T. *International Tables for X-ray Crystallography*; The Kynoch Press: Birmingham, England; 1974; Vol. IV, Table 2.2A.
(26) Ibers, J. A.; Hamilton, W. C. *Acta Crystallogr.* **1964**, *17*, 781.
(27) Creagh, D. C.; McAuley, W. J. In *International Tables for Crystallography*; Wilson, A. J. C., Ed.; Kluwer Academic Publishers: Boston, MA, 1992; Vol. C, Table 4.2.6.8, pp 219−222.
(28) Creagh, D. C.; Hubbell, J. H. In *International Tables for Crystallography*; Wilson, A. J. C., Ed.; Kluwer Academic Publishers: Boston, MA, 1992; Vol. C, Table 4.2.4.3, pp 200−206.

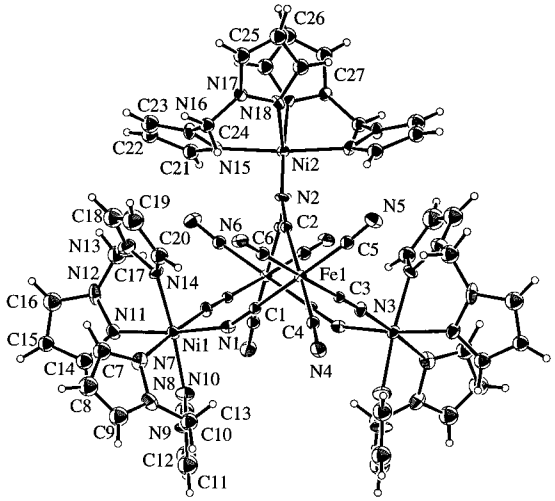

Figure 1. A single cluster of **1**, showing the atom-labeling scheme and 20% probability ellipsoids.

Table 3. Selected Bonding and Nonbonding Distances (Å) and Bond Angles (deg) for **1**

Bonding Distances			
Ni(1)−N(1)	2.07(1)	Ni(1)−N(7)	2.13(1)
Ni(1)−N(10)	2.06(1)	Ni(1)−N(11)	2.14(1)
Ni(1)−N(14)	2.08(1)	Ni(2)−N(2)	2.02(1)
Ni(2)−N(15)	2.10(1)	Ni(2)−N(18)	2.11(1)
Fe(1)−C(1)	1.94(1)	Fe(1)−C(2)	1.96(1)
Fe(1)−C(3)	1.96(1)	Fe(1)−C(4)	1.91(1)
Fe(1)−C(5)	1.92(1)	Fe(1)−C(6)	1.93(2)
N(1)−C(1)	1.16(1)	N(2)−C(2)	1.12(1)
N(3)−C(3)	1.11(2)	N(4)−C(4)	1.15(2)
N(5)−C(5)	1.13(2)	N(6)−C(6)	1.15(2)
Nonbonding Distances			
Fe(1)···Fe(1a)	6.438(4)	Fe(1)···Ni(1)	5.042(3)
Fe(1)···Ni(2)	5.058(2)	Ni(1)···Ni(2)	6.654(3)
Ni(1)···Ni(1a)	7.028(5)	Fe(1)···Fe(1*)[a]	9.576(3)
Angles			
N(1)−Ni(1)−N(7)	91.6(5)	N(1)−Ni(1)−N(10)	96.2(5)
N(1)−Ni(1)−N(3)	89.8(4)	N(1)−Ni(1)−N(11)	172.9(5)
N(1)−Ni(1)−N(14)	87.1(5)	N(7)−Ni(1)−N(10)	86.5(6)
N(11)−Ni(1)−N(14)	85.9(5)	Fe(1)−C(1)−N(1)	178(1)
Fe(1)−C(2)−N(2)	173(1)	Fe(1)−C(3)−N(3)	179(1)
Fe(1)−C(4)−N(4)	175(1)	Fe(1)−C(5)−N(5)	175(1)
Fe(1)−C(6)−N(6)	179(2)	Ni(1)−N(1)−C(1)	155(1)
Ni(2)−N(2)−C(2)	166(1)		

[a] Fe(1*) is in the nearest-neighbor cluster.

There are now three terminal ν(CN) bands at 2128, 2119, and 2110 cm^{-1}, the first being probably due to C−N(4).

Crystal and Molecular Structure of 1. An ORTEP view of the discrete, neutral pentanuclear cluster in **1** is shown in Figure 1. Relevant structural parameters are given in Table 3. The cluster consists of two $[Fe(CN)_6]^{3-}$ moieties connected via three CN−Ni(bpm)$_2$−NC bridges in a *fac* arrangement for each Fe. The Ni atoms have a *cis* geometry. The three remaining CN groups on each Fe are monodentate but are involved in important hydrogen-bonding networks to water molecules (*vide infra*). There are no direct bridges between the Ni atoms, between the Fe atoms, or between clusters. In the recently reported structure of $[Ni(cyclam)]_3[Cr(CN)_6]_2\cdot 20H_2O$, three [Ni(cyclam)] groups also bridge to three CN groups in a *fac* arrangement on an Fe cation, but in this case, the planarity of each [Ni(cyclam)] allows further CN bridging to occur to another $[Fe(CN)_6]^{3-}$ group, via the *trans-axial* portion of each [Ni(cyclam)].[8] A layered array is consequently built up, which is not the case in **1** because of the *cis*-[Ni(bpm)$_2$] blocking effect. A different structural role for Fe occurs in $[Ni(tren)]_3[Fe(CN)_6]_2\cdot 6H_2O$ such that one $[Fe(CN)_6]^{3-}$ group bridges four [Ni(tren)]$^{2+}$ groups, while another bridges only two, thus leading to chain formation.[9] The $[Fe(CN)_6]^{3-}$ bridging modes in $[Ni(en)_2]_3[Fe(CN)_6]_2\cdot 2H_2O$[2] and $\{Ni(pn)_2\}_2[Fe(CN)_6]ClO_4\cdot 2H_2O$[3,29] are different again.

Table 4. Hydrogen Bond Distances (Å) in **1**

O(1)···O(3)	2.85(3)	O(2)···O(3)	2.78(2)
O(2)···O(2a)	2.90(3)	O(2)···N(6)	2.96(2)
O(3)···O(4)	3.08(2)	O(4)···N(4)	2.76(2)
O(4)···N(5)	2.94(2)	O(1)···N(10)	3.09(2)

The key bridging pathways within each cluster of **1** are the *cis*-disposed Fe(1)−C≡N−Ni−N≡C−Fe(1a) linkages. Average M···M. separations within the cluster are Fe···Ni 5.05 Å, Fe···Fe 6.44 Å, and Ni···Ni 6.65−7.03 Å. The geometry around the nickel atoms is octahedral, four nitrogen atoms originating from the two bpm ligands and two from the cyanide groups. Ni−N distances range between 2.06(1) and 2.14(1) Å for the bpm ligands and between 2.02(1) and 2.07(1) Å for nickel cyanide nitrogens. Fe−C−N bond angles are close to linear (175(1)−179(2)°), whereas Ni−N−C angles differ significantly from linearity (155(1)−166(1)°).

The seven water molecules form an intriguing hydrogen-bonded array with each other and with the pentanuclear Ni_3Fe_2 clusters. It can be seen in Figure 2 and Table 4 that a pentagon of water molecules (O(1), O(3), O(2), O(2a), O(3a)) have two water molecules (O(4) and O(4a)) in 1,3-positions. These O(4) and O(4a) oxygens are H-bonded to the N(4) and N(4a) cyanide nitrogens on each $[Fe(CN)_6]^{3-}$ *within* the cluster, thus forming an intramolecular interaction across five or six waters (O(4)···N(4) 2.76 Å).

The water molecules also connect to further clusters via O(4)···N(5) (2.94 Å) and O(2)···N(6) (2.96 Å) interactions, to give a complicated three-dimensional network of H-bonding clusters and water molecules. To simplify matters, we can think of the cluster and the seven-molecule water cage as a single unit (held together by the N(4)···O(4) interactions). This unit lies on a 2-fold axis which passes through Ni(2) and O(1) and relates one half of the unit to the other.

Each unit connects to eight other units via four each of the types of links (O(4)···N(5) (type A) and O(2)···N(6) (type B)) (Figure 2). The type A links connect the units into a diamond-like network (Figure 3a). This is the shortest route between two clusters (N(4)···O(4)···N(5d)). The type B links connect the units into square-grid sheets parallel to the *ab* plane of the crystal (Figure 3b). The sheets stack in the direction of the *c* axis and are related by the 4_3 screw axis. Thus, there are four such sheets per unit cell, each a 90° rotation of the adjoining sheets. The type B links represent a longer connection (N(4)···O(4)···O(3)···O(2)···N(6e)) between clusters than the type A links.

Figure 3c shows the combination of the two types of connections in a schematic form. The circles representing the units are imaginary points on the 2-fold axes halfway between the Ni(2) and O(1) atoms of each unit. The filled bonds represent the diamond network of type A links, while the open bonds represent the square-grid sheets of type B links. The thin lines show the unit cell.

The sheets formed by the type B links also contain a third type of route between clusters (N(6e)···O(2)···O(2a)···N(6i), type C). A three-water route between clusters also exists (N(5d)···O(4)···O(3)···O(2)···N(6e), type D), involving both the diamond and sheet nets. Thus, in order of increasing length, the shortest H-bonding connections between clusters are as

(29) Ohba, M.; Okawa, H.; Ito, T.; Ohto, A. *Chem. Commun.* **1995**, 1545.

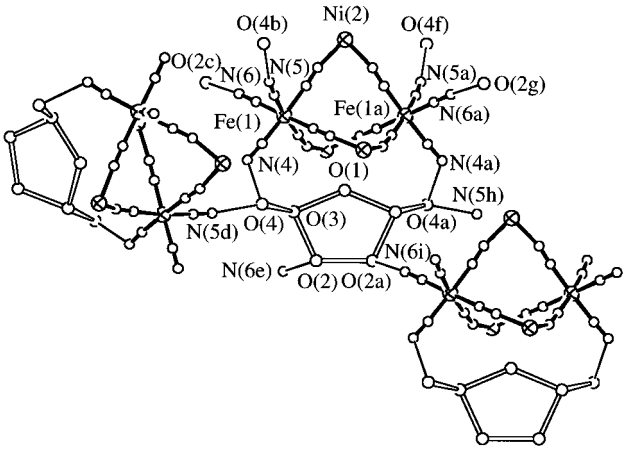

Figure 2. Three cluster-water "units", showing the seven hydrogen-bonded water molecules per cluster. Each unit is held together by O(4)···N(4) H-bonds, and each unit is connected to eight others by H-bonding *via* the water molecules. All H-bonding connections from the central unit are shown, and the two distinct types (O(4)···N(5) and O(2)···N(6)) are highlighted by the inclusion of the whole adjoining unit for one of each type.

follows: one water (type A links), two waters (type C), and three waters (types B and D).

Magnetic Properties. We have studied the temperature dependence of the magnetic susceptibilities in the temperature range 4.2−300 K usually in a field of 1 T. To test for long-range ordering, magnetization measurements were made on the sample by cooling it from *ca*. 35 to 4.2 K in zero field and then warming it in a field of 5 Oe (ZFCM). Field-cooled magnetization measurements (FCM) were made by cooling in a field of 5 Oe. The various measurements of remanent magnetization (RM) are described later and in the Experimental Section. High-field magnetization measurements at fixed temperatures, in the range 2−30 K, were made using fields between 0 and 5 T. Checks were made for any movement (torquing)[19,30] of the polycrystallites in the sample container, and none was found. Hysteresis loops were also measured to confirm magnetic phase transitions. As in the recent work of Ohba and Okawa[12] and of Matsumoto, Floriani, and co-workers,[5] we describe results for slowly grown crystalline aggregates and for rapidly precipitated powder samples of **1**.

(a) Crystalline Samples of 1. Sample 1 consisted of a 3 mg aggregate of small individual crystals each having the structural characteristics described above. A plot of $\chi_M T$ vs temperature in a field of 1 T is shown in Figure 4a. χ_M is the susceptibility per Ni_3Fe_2 unit. The $\chi_M T$ value increases gradually from a plateau value of 5.12 cm^3 K mol^{-1} (6.4 μ_B) between 300 and 100 K to a sharp maximum at 9 K of 10.93 cm^3 K mol^{-1} (9.35 μ_B) before decreasing below this temperature. The same behavior has been reported in "polycrystalline" $[Ni(tren)]_3[Fe(CN)_6]_2 \cdot 6H_2O$[9] and related amino species[2,29] although the field value was not always given. The corresponding $1/\chi_M$ vs temperature plot, shown in Figure 4b, follows Curie−Weiss behavior with a Weiss constant, Θ, of + 6 K, indicative of ferromagnetic coupling within the Ni_3Fe_2 cluster of **1**. This arises due to the orthogonality of the magnetic orbitals on $Ni^{II}(t_{2g}^6e_g^2)$ and $Fe^{III}(t_{2g}^5)$. The data of Figure 4 are compatible with a ground state $S = 4$ resulting from such intramolecular ferromagnetic coupling with $g_{Ni} \approx 2.3$ and $g_{Fe} \approx 2.2$. However, variation of the applied field, above and below 1 T, shown in Figure 5, leads to some surprises. Above 1 T, the value of

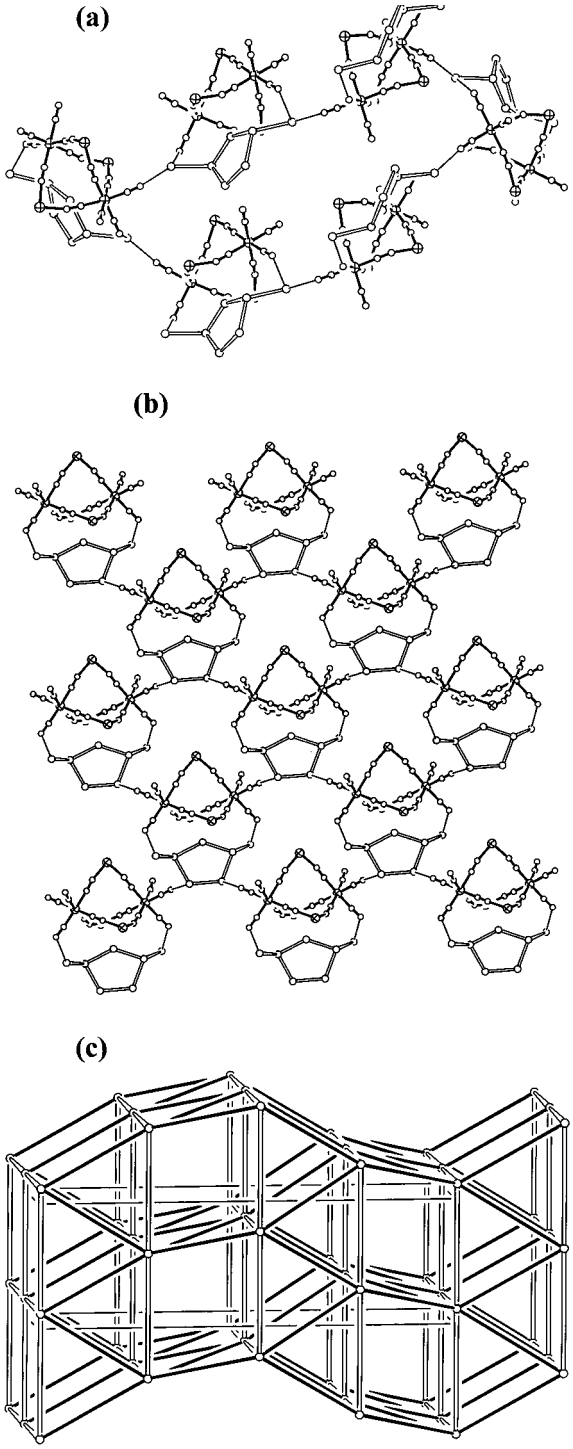

Figure 3. (a) A ring of six connected units in the diamond-like net defined by the type A links. (b) A sheet of units defined by the type B links. (c) A schematic depiction of the connections between units. The circles represent the units, with the filled bonds representing the diamond-like network of type A links and the open bonds representing the square-grid sheets of type B links. The thin lines show the unit cell.

$\chi_M T$(max) decreases, reaching 10.04 cm^3 K mol^{-1} (8.96 μ_B) at 1.5 T. The $\chi_M T$ data for fields of 1−1.5 T are identical in the range 20−100 K. Below 1 T, the value of $\chi_M T$(max) increases dramatically, reaching 37.42 cm^3 K mol^{-1} at 100 Oe and 90.48 cm^3 K mol^{-1} at 5 Oe (not shown), with corresponding sharp increases in the value occurring below 20 K. These $\chi_M T$ values are well above that expected for an isolated $S = 4$ pentanuclear cluster of 10.00 cm^3 K mol^{-1}. Such behavior is strongly suggestive of three-dimensional magnetic ordering occurring,

(30) Kennedy, B. J.; Murray, K. S. *Inorg. Chem.* **1985**, *24*, 1552.

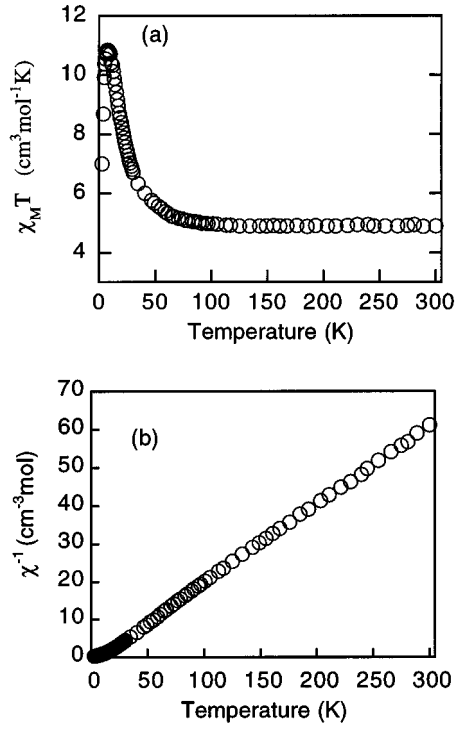

Figure 4. (a) Plot of $\chi_M T$, per molecule unit, versus temperature for crystalline sample 1 of complex **1**. (b) Corresponding plot of χ^{-1}. Applied field = 1 T.

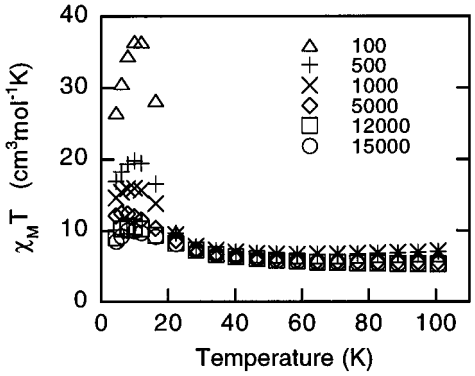

Figure 5. Plots of $\chi_M T$ versus temperature for sample 1 of **1**. Applied-field values are shown in oersteds.

i.e., a magnetic phase transition. It should be noted that the use of $\chi_M T$ in the region of T_c is qualitatively useful and illustrative. The magnetization data should strictly be plotted.

The values of $\chi_M T$ in the temperature range 20−100 K are not identical when applied-field values, 1000, 500, and 100 Oe are used, the lower fields leading to a broad minimum in $\chi_M T$ at *ca*. 60 K. There is no such broad minimum at field values of 5000 Oe and above. The temperature dependence of $\chi_M T$ in the $\chi_M T$(max) region, as a function of field, is reminiscent of that observed for other small ferromagnetically coupled isolated clusters in which the energies of low-lying Zeeman (M_s) levels vary sensitively with field and temperature.[1] It is also somewhat similar to data reported for 2D-layer "Kagome" lattice compounds of the type $CuX_2(cpa)_6$, where X = F, Cl, or Br and cpa = carboxypentonic acid.[31]

In order to probe further the nature of long-range ordering in this crystalline sample of **1**, magnetization data were recorded in the low-temperature region. Figure 6 shows the plots of FCM, ZFCM, and RM (remanent magnetization) versus temperature. The FCM and ZFCM data diverge below *ca*. 23 K,

(31) Maruti, S.; ter Haar, L. W. *J. Appl. Phys.* **1994**, *75*, 5949.

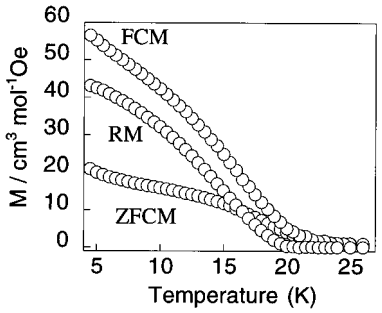

Figure 6. Plots of field-cooled (FCM), zero-field-cooled (ZFCM), and remanent magnetization (RM) versus temperature for sample 1 of **1**. Applied field = 5 Oe.

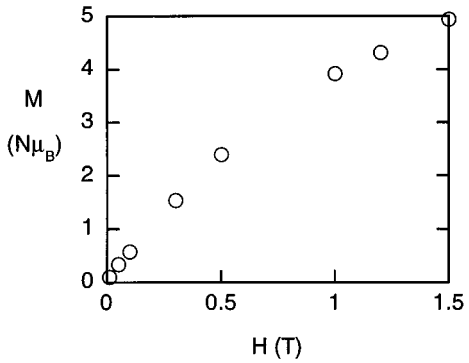

Figure 7. Magnetization, *M*, versus field, *H*, for sample 1 of **1** at 4.5 K.

the FCM continuing to increase gradually between 20 and 4.2 K while the ZFCM data in this region approach a plateau value, lower than that of the FCM, it also crosses the RM values at *ca*. 16 K. The RM vanishes at *ca*. 21 K and has a value of 42 cm^3 mol^{-1} Oe at 4.2 K. The slope of the FCM values below T_c is less sharp than for the $[Ni(tren)]_3[Fe(CN)_6]_2 \cdot 6H_2O$ and $K[Mn(3MeO\text{-}salen)]_2[Fe(CN)_6]$ magnets.[5,9]

The magnetization versus field (0−1.5 T) plot extracted from Figure 5, at 4.5 K, is given in Figure 7. There are no rapid changes in shape or sigmoidal shapes in the low-field region of the kind noted, respectively, for the ferrimagnet $[Ni(tren)_3][Fe(CN)_6] \cdot 6H_2O$[9] or the metamagnet $K[Mn(3\text{-}MeO\text{-}salen)]_2[Fe(CN)_6]$.[5] In attempting to define the nature of magnetic ordering from the *M* vs *H* data, we note that the sharp increase in *M* at very low fields, typical of ferromagnetic ordering, is not evident in Figure 7 in the way it is, for instance, for the compound $[Mn^{II}Cu^{II}(obze)(H_2O)_2]$ [obze = *N*-(2-carboxyphenyl)-*N*′-(carboxymethyl)oxamido(4−) (trivially named oxamido-*N*-benzoato-*N*′-ethanato)] reported by Kahn *et al.*[13] The magnetization data for a larger crystalline sample (sample 2) were explored in higher fields and are compatible with those of sample 1 (*vide infra*); they are similar to those found for crystalline $[Mn(saltmen)_4][Fe(CN)_6](ClO_4) \cdot H_2O$ (saltmen = *N*,*N*′-(1,1,2,2-tetramethylethylene)bis(salicylideneaminato)), which has a 2D-network structure consisting of cyclic dodecameric [...Mn−NC−Fe−CN−Mn...]$_4$ units and which was concluded to be ordered ferromagnetically.[5]

The second 14.07 mg crystalline sample of **1**, sample 2, was ground finely prior to the measurements being made in the SQUID instrument. Very small crystallites still persisted after grinding. The temperature dependence of $\chi_M T$ vs *T* in a 1 T field is identical to that shown in Figure 4. Likewise, the temperature dependence of the magnetization data, in a 5 Oe field, is similar to that of sample 1 in both shape and size. One small difference is the temperature, 26 K, at which the FCM and ZFCM data diverge. Since samples 1 and 2 have identical

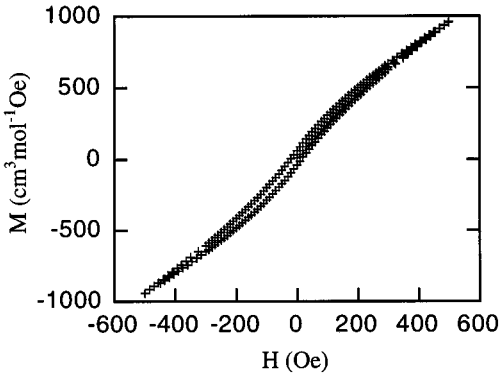

Figure 8. Hysteresis loop for crystalline sample 2 of **1** at 10 K.

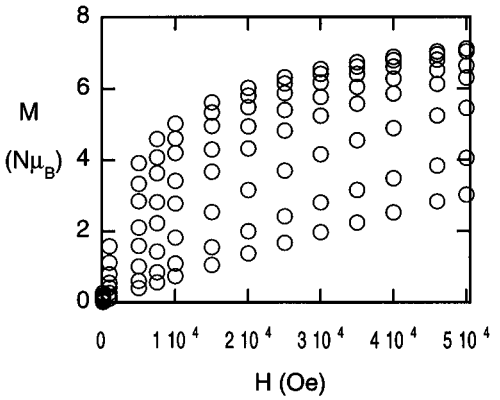

Figure 9. High-field magnetization isotherms for sample 2 of complex **1**. Temperatures, from top to bottom: 2, 3, 4, 5.5, 7, 10, 15, 20 K.

structures, the difference noted in T_c presumably relates to the size of the crystallites.

The hysteresis loop at 10 K for sample 2 is shown in Figure 8 and displays behavior reasonably characteristic of a ferromagnet with a coercive field of about 20 Oe and a remanent magnetization of 50 cm^3 mol^{-1} Oe. The small value of the coercive field is similar to that found for the Ni(tren) derivative, in which it was ascribed to small magnetic anisotropy as well as the absence of irreversible movements of domain walls.[9]

Variable-field magnetization isotherms (100 Oe to 5 T) for sample 2 are shown in Figure 9. The magnetization values do not fully saturate to the expected $S = 4$ value of 8 $N\mu_B$ for this five-spin (three S_{Ni}, two S_{Fe}) system in the lowest temperature (2 K)−highest field (5 T) combination used but are close to it, *viz.*, 7.2 $N\mu_B$. Such divergences are not uncommon and probably relate to small zero-field splittings on the Ni^{II} centers within the Ni_3Fe_2 clusters. As in the Mn^{III}saltmen−Fe(CN)$_6$ and Mn^{II}Cu^{II} oxamate systems, the magnetization saturates more easily as the temperature decreases, in agreement with ferromagnetic ordering.[32,33]

(b) Rapidly Precipitated Powder Samples of 1. Seven samples were prepared in water and investigated. Sample 3, for example, was made by rapid precipitation, as described earlier, and was shown to be isostructural with the single crystals of **1** by use of XRD measurements. The Mössbauer spectrum at 77 K shows a single sharp doublet with parameters $\delta = -0.05$ mm s^{-1} and $\Delta E_Q = 0.82$ mm s^{-1}, typical of $[Fe(CN)_6]^{3-}$-containing species in a unique structural environment. Related values[34] for $[Fe^{III}(CN)_6]^{3-}$ are $\delta = 0.0$ mm s^{-1} and $\Delta E_Q =$ 0.47 mm s^{-1}. The negative value of the isomer shift has been noted by us in other molecular magnets and discrete clusters containing $[Fe(CN)_6]^{3-}$ bridging groups.[35] The size of the quadrupole splitting reflects the asymmetry around the low-spin Fe^{III} centers.

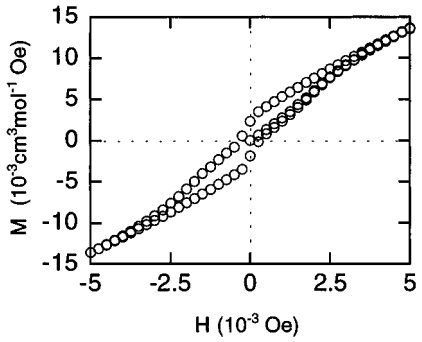

Figure 10. Hysteresis loop for powder sample 3 of **1** at 5 K.

The magnetic data for sample 3 were reproducible after standing for a 6 month period. Low-field plots of FCM, ZFCM, and RM versus temperature have been published earlier.[1] The T_c value is the same as that found for the crystalline sample 1. In comparison to the case of sample 1, the ZFCM plot for sample 3 shows the usual maximum at temperature T_c but the values plateau out to a nonzero value at temperatures below T_c. The $\chi_M T$ vs temperature data in a 1 T field were also given in ref 1, and they are similar to those shown in Figure 4a. In a tiny field of 1 Oe, the $\chi_M T$ values increase sharply from a temperature of *ca*. 21 K, reaching a maximum value of 1035 cm^3 K mol^{-1} at 14 K before decreasing rapidly toward 421 cm^3 K mol^{-1} at 4.2 K. This is similar to the behavior of the crystalline sample and indicative of long-range ordering occurring. Between 21 and 300 K, there is a very shallow minimum in $\chi_M T$ at *ca*. 50 K, but the $\chi_M T$ values are essentially independent of temperature. Confirmation of magnetic ordering is given by the hysteresis loop measured at 5 K and shown in Figure 10. This yields a coercive field value of 333 Oe and remanent magnetization of 1478 cm^3 mol^{-1} Oe. The shape of the loop is similar to that displayed by the ferromagnet [Mn(saltmen)]$_4$[Fe(CN)$_6$]ClO$_4$.[5] A series of high-field magnetization isotherms (4.2−24 K) are similar in shape to those of sample 1 shown in Figure 7.

The other powder samples showed magnetic ordering similar to that of sample 3 except in two cases, where no ordering was observed. All the powder samples showed compositions, IR spectra, and XRD patterns similar to each other and to those of the crystalline samples. Variations in the method of sample filtration and in the mole ratio of reagents used were not able to identify the precise origin of these sample-dependent differences. Ohba and Okawa[12] noted differences in magnetic ordering for rapidly precipitated samples of $[Ni(en)_2]_3[Fe(CN)_6]_2 \cdot 2H_2O$ when variations were made in the concentrations of reagents and the temperature used for syntheses. In distinction to that of **1**, their crystalline sample showed no long-range ordering. However, it was prepared by a route different from the one used for the powder sample. They proposed that the extended "rope−ladder" structure of the crystals[2] may not have completely formed in the rapidly precipitated powders, thus leading to quasi-two- and three-dimensional domains in the lattice which are not identifiable by XRD comparisons. If similar arguments apply here, the differences in the hydrogen-bonded water network structure might be anticipated from

(32) Kahn, O. *Molecular Magnetism*; VCH: Weinheim, Germany, 1993.
(33) Kahn, O.; Pei, Y.; Verdaguer, M.; Renard, J. P.; Sletten, J. *J. Am. Chem. Soc.* **1988**, *110*, 782.
(34) Greenwood, N. N.; Gibb, T. C. *Mössbauer Spectroscopy*; Chapman and Hall: London, 1971.
(35) Parker, R. J.; Hockless, D. C. R.; Moubaraki, B.; Murray, K. S.; Spiccia, L. *Chem. Commun.* **1996**, 2879.

sample to sample. In neither the $Ni(bpm)_2$ nor the $Ni(en)_2$ case is the magnetic ordering under total preparative control except in crystals of **1**, which are magnetically and structurally reproducible.

The Role of the Hydrogen-Bonded Water Cluster in 1. Working on the assumption that the hydrogen-bonded water groups provide important exchange pathways between the Ni_3-Fe_2 clusters, we carefully dehydrated a portion of sample 3 by heating, under nitrogen, at 200 °C for 36 h, before sealing the container and rapidly transferring it to the sample chamber of the SQUID instrument. In contrast to the hydrated parent material, the dehydrated sample displayed no magnetic ordering in a field of 5 Oe. The FCM and ZFCM data were identical in the region 5−25 K. The temperature dependence of $\chi_M T$ over the range 4.2−300 K, in a field of 1 T, was similar in shape to that displayed in Figure 4a, but the $\chi_M T$(max) value at 7.1 K was lower, *viz*. 8.35 cm^3 K mol^{-1} (8.17 μ_B). The values between 100 and 300 K were temperature independent at 5.28 cm^3 K mol^{-1} (6.50 μ_B). This behavior, for the anhydrous material, is that anticipated for an isolated pentanuclear cluster undergoing intramolecular ferromagnetic coupling. Complex **1** therefore provides a rare, clear-cut case of long-range magnetic ordering being propagated by H-bonded water pathways, probably by means of a spin polarization mechanism. A few other reports have implicated H-bonded water pathways in intermolecular ferromagnetic coupling.[8,13,36]

The Nature of the Magnetic Transition in Ordered Samples of 1. Thus far, the various magnetic measurements have largely pointed to long-range ferromagnetic ordering occurring. The M_{sat} value is close to that expected for a ferromagnetically coupled $\{(S = 1)_3(S = {}^1/_2)_2\}$ five-spin system. The high-field magnetization isotherms and the hysteresis loop, while not ideal in shape for ferromagnetizm, do compare well to those of other purported soft ferromagnets, rather than to those of ferri- or metamagnets. The very shallow minimums in μ_{eff} observed at $T > T_c$, in fields of < 0.1 *T*, while reminiscent of antiferromagnetic systems of Kahn's MnCu oxamide type,[33] do not appear in applied field values of magnitude greater than 0.1 T. Perhaps some domain effects still persist in low fields at temperatures of $T > T_c$.

Another possible alternative explanation for the proposed magnetic order in **1** is spin-glass formation. These materials are commonly found[37] in conducting d-block metal alloys, of varying mole ratios, and in inorganic insulators such as $Zn_{1-x}Fe_xF_2$, with few examples known of large bimetallic coordination compounds of the present type. One celebrated example which shows some spin-glass characteristics is the amorphous semiconductor $V(TCNE)_2 \cdot 0.5\ CH_2Cl_2$ (TCNE = tetracyanoethylene), with a magnetic transition temperature well above 300 K.[38] Another amorphous (insulating) example is $Co^{II}{}_3(BTCA)_2 \cdot 6H_2O$ ($BTCA^{3-}$ = 1,3,5-benzenetricarboxylate) which has a freezing temperature of 23 K and some, but not all, characteristic features of a spin-glass.[39] The structures of these two materials are not known. The dodecanuclear complex $[Mn_{12}O_{12}(O_2CPh)_{16}(H_2O)_4]$ shows a few properties typical of a spin-glass, such as spin frustration, but this assignment was rejected in view of the lack of randomness in such a highly crystalline compound.[19] Spin-glasses have a cooperative nature in the frozen state, below the freezing temperature T_f, and are characterized by a number of properties; these include randomness (e.g., in positions of spins or in signs of neighboring coupling), disorder (e.g., in lattice site or bond; otherwise, ferromagnetic or antiferromagnetic long-range ordering would occur), mixed or competing exchange interactions (here they would be of the superexchange type or occur via H-bonded water interactions), and frustration—which arises from a combination of randomness and mixed exchange interactions. There is considerable controversy as to whether disorder is actually needed for frustration of spins to occur. These features lead to properties such as macroscopic anisotropy and various time- and age-dependent metastabilities in applied magnetic fields and in the temperature range $T < T_f$. At temperatures $T > T_f$, spin-glass materials possess "building blocks" of spin which display local correlations or "clusters", with short-range order, usually ferromagnetic.

Experimentally, there is a wide array of measurements capable of identifying the spin-glass state;[37,40] these include magnetization, hysteresis, specific heat, and neutron scattering. We have performed a number of experimental magnetization measurements, separate from those already described to determine whether spin-glass rather than ferromagnetic ordering is responsible for the magnetic phase transition. Powder sample 3 was mainly used. The plotted data are not given here but are available in the Supporting Information. They include plots of ln(*M*) vs ln(*H*), thermal remanent magnetization (TRM) and isothermal remanent magnetization (IRM) vs field, and remanent magnetization (RM) vs time (ln(*t*)). None of these measurements yield data characteristic of spin-glass behavior. Furthermore, the hysteresis loop for sample 3, when cooled in a field of 5 Oe down to 5 K, is similar to that shown in Figure 10. It does not display any displacement along the field axis, which would be expected for a spin-glass.[37]

The experimental data, therefore, militate against spin-glass formation. Consideration of the Mydosh (structural/randomness/frustration) categorization of spin-glasses[37] leads to conclusions that $Ni^{II}{}_3Fe^{III}{}_2$ "building blocks" in complex **1** are not random or disordered nor do they grow in size with decreasing temperature. The spins from these building blocks would not be expected to align randomly as the temperature is decreased, since the interconnecting H-bonded water moieties have a well-defined, nonrandom geometry. Spin frustration probably does occur within the $Ni^{II}{}_3Fe^{III}{}_2$ cluster of **1** (see below), and it may be feasible between the clusters in the lattice structure owing to the different H-bonded water pathways which exist.

In summary, considerable efforts have been made to identify, unambiguously, the nature of the magnetic transition occurring at *ca*. 23 K in ordered samples of **1**. The bulk of the experimental data favors long-range ferromagnetic ordering, but some of the magnetization data do not give ideal behavior. However, for molecular magnets of the present general kind, what is representative of "ideal" behavior has yet to be worked out. We are currently exploring the isostructural Co^{II} analog of **1**, *viz*. $[(Co^{II}(bpm)_2)_3(Fe(CN)_6)_2] \cdot 7H_2O$ to determine whether T_c and other properties of the ordered phase depend on M^{II} in the M(bpm) fragment and hence on the spin of the pentanuclear cluster.[41]

(36) Drljaca, A.; Hockless, D. C. R.; Moubaraki, B.; Murray, K. S.; Spiccia, L. *Inorg. Chem.* **1997**, *36*, 1988.
(37) (a) Mydosh, J. A. *Spin Glasses. An Experimental Introduction*; Taylor and Francis: London, 1993. (b) Mydosh, J. A. *J. Magn. Magn. Mater.* **1996**, *157/158*, 606.
(38) Zhou, P.; Morin, B. G.; Miller, J. S.; Epstein, A. J. *Phys. Rev. B* **1993**, *48*, 1325.
(39) Landee, C. P.; Wynn, C. M.; Albrecht, A. S.; Zhang, W.; Vunni, G. B.; Parent, J. L.; Navas, C.; Turnbull, M. M. *J. Appl. Phys.* **1994**, *75*, 5535.
(40) O'Connor, C. J. In *Molecule-Based Magnetic Materials*; Turnbull, M. M., Sugimoto, T., Thompson, L. K., Eds.; ACS Symposium Series 644; American Chemical Society: Washington, DC, 1996; Chapter 4, pp 44−66.
(41) Gilligan, N.; Moubaraki, B.; Van Langenberg, K.; Murray, K. S. Unpublished data.

Exchange-Coupling Scheme within the Ni_3Fe_2 Cluster of the Anhydrous Sample of 1. The absence of long-range ordering in the anhydrous sample of **1** has allowed us to probe the intramolecular coupling scheme in some detail. We have used a Heisenberg Hamiltonian approach similar to that given recently for other penta- and tetranuclear complexes.[1,32,42,43] The Hamiltonian appropriate to the isolated Ni_3Fe_2 cluster structure shown in Figure 1 is given in eq 1. S_1, S_2, and S_3 are the spins

$$H_{ex} = -2J_1(\mathbf{S}_1\cdot\mathbf{S}_4 + \mathbf{S}_1\cdot\mathbf{S}_5 + \mathbf{S}_2\cdot\mathbf{S}_4 + \mathbf{S}_2\cdot\mathbf{S}_5 + \mathbf{S}_3\cdot\mathbf{S}_4 + \mathbf{S}_3\cdot\mathbf{S}_5) - 2J_2(\mathbf{S}_1\cdot\mathbf{S}_2 + \mathbf{S}_1\cdot\mathbf{S}_3 + \mathbf{S}_2\cdot\mathbf{S}_3) - 2J_3(\mathbf{S}_4\cdot\mathbf{S}_5) \quad (1)$$

of Ni^{II}, and S_4 and S_5 are the spins of Fe^{III} (low spin). $J_1 = J_{NiFe}$; $J_2 = J_{NiNi}$; $J_3 = J_{FeFe}$. The summation vector coupling expressions $\mathbf{S}' = \mathbf{S}_1 + \mathbf{S}_2$, $\mathbf{S}_A = \mathbf{S}' + \mathbf{S}_3$, $\mathbf{S}_B = \mathbf{S}_4 + \mathbf{S}_5$, and $\mathbf{S}_T = \mathbf{S}_A + \mathbf{S}_B$ were used to calculate respective spin states and their energies. This leads to 26 spin states with $S_T = 0$, 1, 2, 3, 4 and a total spin degeneracy of 108. The g values for the spin states were calculated from individual ion g values using the relationship in (2) and the expressions given for the coefficients α and β:

$$g_T = \alpha g_{Ni} + \beta g_{Fe} \quad (2)$$

where

$$\alpha = [S_T(S_T + 1) + S_A(S_A + 1) - S_B(S_B + 1)]/\gamma$$

$$\beta = [S_T(S_T + 1) - S_A(S_A + 1) + S_B(S_B + 1)]/\gamma$$

$$\gamma = 2S_T(S_T + 1); \quad \text{if } \gamma = 0, \text{ then } \alpha = 1 \text{ and } \beta = 0$$

The expression for the energies of the various S_T states is

$$E_{total} = E_1 + E_2 + E_3$$

where

$$E_1 = -J_{NiNi}[S_A(S_A + 1) - 3S_{Ni}(S_{Ni} + 1)]$$

$$E_2 = -J_{FeFe}[S_B(S_B + 1) - 2S_{Fe}(S_{Fe} + 1)]$$

$$E_3 = -J_{NiFe}[S_T(S_T + 1) - S_A(S_A + 1) - S_B(S_B + 1)]$$

Magnetic susceptibilities were calculated either in closed form by use of the thermodynamic equation[8] or by diagonalization of the 108 × 108 matrix formed when H_{Zeeman} is added to eq 1. The g values calculated by both approaches were identical.

In approaching the fitting of the $\chi_M T$ versus T data, we see that the high-temperature plateau $\chi_M T$ value of 5.28 cm^3 K mol^{-1} (6.50 μ_B) requires a g value of 2.38 when weak coupling is assumed. The $\chi_M T$(max) value of 8.35 cm^3 K mol^{-1}, at 7.1 K, is between that anticipated for an isolated $S_T = 3$ state (6.00 cm^3 K mol^{-1}, $g = 2.0$) and that for an $S_T = 4$ state (10.00 cm^3 K mol^{-1}, $g = 2.0$). A g value of *ca.* 2.38 is required to give the $\chi_M T$(max) value for an $S_T = 3$ state whereas a g value of much less than 2 would be required for $S_T = 4$. While such an average g value is rather high, it is not unknown for octahedral Ni(II) and Fe(III) (low spin). The correlation diagram of relative energies of spin states versus the ratio $\alpha = J_{NiNi}/J_{NiFe}$ (assuming $J_{FeFe} = 0$) shows that this ratio lies between −0.33 and −0.5 for $S_T = 3$ being the ground state and at > -0.33 for $S_T = 4$. It is important to note that the turnover in the $\chi_M T$ values at 7.1 K derives largely from the effect of theapplied magnetic field and the consequent depopulation of low-lying Zeeman levels. Zero-field-splitting effects also contribute (see later). The common practice of assuming an intercluster antiferromagnetic coupling is not required.

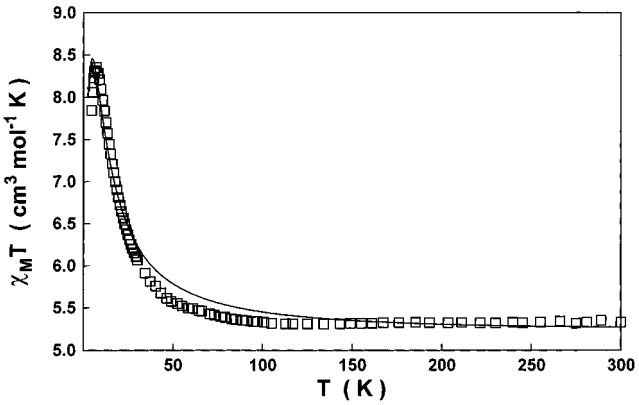

Figure 11. Plot of $\chi_M T$ versus temperature for the dehydrated sample of **1**. The solid line is the best-fit calculated curve using the parameters $g_{Ni} = 2.38$, $g_{Fe} = 2.15$, $J_{NiFe} = 5.36$ cm^{-1}, $J_{NiNi} = -1.7$ cm^{-1}, $J_{FeFe} = 0$, and TIP = 200 × 10^{-6} cm^3 mol^{-1}.

A detailed exploration of parameter space was carried out during the fitting of the 1 T plot of $\chi_M T$ vs T. Some conclusions are (i) J_{NiFe} is small (<6 cm^{-1}) and positive and (ii) the ratio α is close to the crossover point of the $S_T = 3$ and $S_T = 4$ states, *viz.* −0.33. If α is assumed to be > -0.33 or positive (for $S_T = 4$), then $\chi_M T$(max) and $\chi_M T$(300 K) values cannot be fitted simultaneously. We also conclude that the temperature of the maximum in $\chi_M T$ is rather insensitive to variation in J_{NiNi}, for a fixed J_{NiFe}, but the size of $\chi_M T$ changes sensitively. The best fits to the data were found when we used the parameter values of $g_{Ni} = 2.38(1)$, $g_{Fe} = 2.20(5)$, $J_{NiFe} = 5.3(1)$ cm^{-1}, and $J_{NiNi} = -1.7(3)$ cm^{-1} and a temperature-independent susceptibility of ∼200 × 10^{-6} cm^3 mol^{-1}. Observed and calculated data are shown in Figure 11. The region 40−120 K gives moderate agreement while the low- and high-temperature regions are quite good. It should be noted that the ratio of the J values given above leads to an energy separation of only *ca.* 0.5 cm^{-1} between $S_T = 4$ and $S_T = 3$. Herold and Lippard[42] recently noted similar spin frustration effects in a pentanuclear Fe(II)−Kemp's triacid derivative and indicated the need to make magnetization studies at low temperature to determine S_T-(ground). We have done this for the present anhydrous compound in two separate experiments. First, eight isotherms of M vs H were measured on a powdered sample between 2 and 20 K, at fields of 0.01, 0.1, 0.5, 0.75, 1.0, 1.5, 2,0, 2.5, 3.0, 3.5, 4.0, 4.5, and 5.0 T. The plots were similar to those in Figure 9, with the 2 K data reaching a near-saturation value of 7 $N\mu_B$ at 5 T. Use of a Brillouin $S_T = 3$ function, with $g = 2.38$, gave a reasonable fit to all isotherms, one which was certainly superior to that using $S_T = 4$ (Figure S4, Supporting Information). However, the M values at 2 K were lower than those calculated, in the range of fields greater than 1 T. Use of a g value of 2.29 gave good agreement in all fields. This discrepancy is probably due to the neglect of zero-field splitting and/or to the $S_T = 4$ state lying close in energy to $S_T = 3$, which will lead to crossing of Zeeman levels and limitations in Brillouin theory. When attempts were made to calculate the isotherms at 2, 4, 10, and 15 K by use of the Heisenberg exchange model, described above, there was reasonably good agreement at fields <1 T in all cases and at all fields for the 10 and 15 K data. The calculated M values at 2 and 4 K, particularly for fields above 1 T, were larger than the observed

(42) Herold, S.; Lippard, S. J. *Inorg. Chem.* **1997**, *36*, 50.
(43) Murray, K. S. *Adv. Inorg. Chem.* **1995**, *43*, 261.

values. These discrepancies largely mirror the quality of fit obtained at low temperatures in the $\chi_M T$ vs T plot at 1 T (Figure 11). They are again probably indicative of the neglect of zero-field splitting on Ni(II) centers, the effect of which may be difficult to separate from exchange coupling contributions at low temperatures. In a second experiment, the multifield saturation magnetization protocol of Day[44] was employed using fields of 0.2, 1.5, 3.0, and 5.0 T and temperatures between 2 and 20 K. Spin Hamiltonian analysis of the four data sets, using the program WMAG,[45] gave excellent fits using either $S_T = 3$ or $S_T = 4$ but with g values too low ($\sim$1.88) to be sensible for $S_T = 4$. The unique set of best-fit parameters is as follows: $S_T = 3$, $g = 2.38$, $D = 2.4$ cm^{-1}, $E/D = 0.1$ cm^{-1} (Figure S5, Supporting Information). D values of this magnitude are normal for axially distorted Ni(II) species.[32]

In summary, the detailed susceptibility and magnetization vs field studies of the anhydrous complex of **1** show that spin frustration is occurring owing to competing ferromagnetic {Ni(N≡C)Fe} and antiferromagnetic {Ni(N≡C)Fe(C≡N)Ni} pathways, the J values both being small. The best-fit value of the ratio J_{NiNi}/J_{NiFe} shows that the $S_T = 3$ and $S_T = 4$ levels are very close in energy. Interpretation of magnetization isotherms, at very low temperatures, is not straightforward, but favors the $S_T = 3$ level as being the one lowest in energy and undergoing zero-field splitting.

Acknowledgment. This work was supported by a grant from the Australian Research Council to K.S.M. The award of a Commonwealth Scholarship to K.V.L. is gratefully acknowledged. The authors thank Associate Professor J. D. Cashion and Mrs. J. Brown for Mössbauer data, Mr. R. Mackie for X-ray powder diffractograms, and Dr. L. Spiccia for helpful discussions.

Supporting Information Available: Magnetization plots for complex **1**, Figures S1−S3 (ln(M) vs ln(H); thermal and isothermal remanent magnetization vs field; remanent magnetization vs time), and magnetization and (M/H)T plots for a dehydrated sample of **1**, Figures S4 and S5 (6 pages). An X-ray crystallographic file, in CIF format, is available on the Internet only. Ordering and access information is given on any current masthead page.

IC970160K

(44) Day, E. P. *Methods Enzymol.* **1993**, *227*, 437.

(45) Kent, T. A. *WMAG: Magnetization Saturation Data Analysis Software*; WEB Research Co.: Minneapolis, MN, 1995.